Tip-on-Tip Interaction Noise Modeling for Distributed Propellers

Alessandro Zarri[1,4], Frits de Prenter[2], Damiano Casalino[2], Francesco Avallone[3] and Daniele Ragni[2]

[1]Aeronautics and Aerospace Department, von Karman Institute for Fluid Dynamics, Chaussée de Waterloo 72, 1640 Rhode-St-Genèse, Belgium
[2]Department of Flow Physics and Technology, Delft University of Technology, 2629 HS Delft, The Netherlands
[3]Department of Mechanical and Aerospace Engineering, Politecnico di Torino, 10129 Torino, Italy
[4]*alessandro.zarri@vki.ac.be*

Abstract

We propose a modeling approach to predict unsteady-loading tonal interaction noise resulting from the proximity between propellers in distributed-propulsion conditions. Our methodology involves approximating propeller slipstreams as rigid helical vortex paths and computing induced velocity fields using the Biot-Savart law. By modeling unsteady thrust distributions, we apply a rotating dipole formulation to predict sound pressure level directivities. Validation against high-fidelity simulations demonstrates the potential of our approach, although some differences in amplitude exist. Future improvements will focus on incorporating actual lift and drag coefficients for more accurate thrust distributions. Despite its simplifications, our model provides a first step into providing a valuable tool for early-phase concept design, allowing designers to quickly estimate tonal noise contributions in various configurations.

1 Introduction

Distributed propulsion systems have emerged as promising solutions in the sector of urban air mobility (UAM), offering significant potential for enhancing performance while mitigating environmental impacts. As cities face increasing demands for efficient and sustainable transportation solutions, the aviation sector is compelled to explore innovative propulsion technologies to meet these challenges [6]. Among these advancements, Distributed Electric Propulsion (DEP) has garnered considerable attention for its ability to address key objectives such as noise reduction [11]. The concept of DEP entails the distribution of propulsion units throughout the aircraft structure, decoupling the location of power generation from where it is converted into thrust. By dispersing propellers along the wingspan, DEP systems exhibit enhanced propulsive efficiency and reduced community noise levels [3, 18, 1]. This configuration not only augments lift spanwise but also enhances low-speed performance [8, 9]. Moreover, the utilization of electric motors to drive these propellers paves the way for greater energy sustainability, facilitating the realization of futuristic aircraft designs exemplified by initiatives like the Helios Prototype Flying Wing developed by NASA [20]. However, the implementation of DEP systems in urban environments is hindered by the challenge of managing sound emissions, which constitute a significant constraint to the growth of the UAM sector. Studies have shown that when propellers operate in close proximity, complex aerodynamic and acoustic interactions occur, leading to increased sound emissions [10]. These interactions, particularly evident during forward-flight conditions, result in the deformation and interaction of slipstreams, exacerbating both tonal and broadband noise components [23, 22, 26]. Consequently, there is a pressing need to understand the mechanisms underlying sound generation in propeller-based systems and to develop effective noise control strategies to facilitate the integration of DEP technologies into urban airspace. One such strategy involves manipulating the relative phase angle between propellers to achieve partial cancellation of sound emissions through destructive interference [14, 13, 25]. Although promising, the effects of unsteady aerodynamic interactions on sound radiation remain largely unexplored, particularly in forward-flight conditions [5]. Two mechanisms of sound generation are always

present: thickness noise and steady loading noise, which are inherently linked to aerodynamic performance and the kinematics of blade rotational motion. For these mechanisms, models are available in the literature to predict noise using the Blade Element Momentum Theory (BEMT), such as the one used in Ref. [24]. However, as specified by Roger and Moreau [15], as soon as the flow impinging on the blades is non-uniform due to the installation of the propeller in its working environment, the unsteady loading noise mechanism often becomes dominant in several emission directions. This may hold true for both broadband and tonal sound mechanisms. In this work, however, we disregard the former and specifically focus on developing a model capable of predicting tonal interaction noise due to the proximity between propellers operating in DEP conditions. The goal of this research path is to develop a fast and simple prediction method capable of estimating the increase in this type of noise without necessarily relying on high-fidelity simulation and starting from the same input data as the BEMT-based methods estimating thickness and steady-loading noise mentioned above. In this work, a strategy is proposed to model the unsteady interaction between propellers for estimating the required inputs to compute the unsteady loading noise. To compare the modeled results, the simulations conducted in Ref. [24] are exploited.

2 Methodology

2.1 High-fidelity simulations: array of propellers

The computational setup for this study is based on experiments conducted by de Vries *et al.* [5], which involved a configuration with three adjacent propellers. The propellers used in the experiment, known as TUD-XPROP-S propellers, feature six blades with a radius (R) of $0.1016\,\mathrm{m}$. The geometric details of these propellers, including the pitch angle and chord distributions along the blade span, were provided by Delft University of Technology [5]. High-fidelity simulations of this setup were carried out by Zarri *et al.* [24]. These simulations are used as a basis to build the low-fidelity technique proposed in this work. Hereafter, key points regarding the computational setup are described, and more details are given in the original paper. While replicating the spinner and blade geometries exactly from the experiments, certain components such as the wind-tunnel test section and supports holding the nacelles in place were excluded from the computational domain. The nacelles were designed with a length corresponding to $3.7R$ and tapered termination to minimize flow disturbance around the rotors. Three identical propellers were distributed along the Y-axis with a tip clearance of $\delta = 0.02D = 4.064\,\mathrm{mm}$, illustrated in Figure 1(a). The configuration studied here features the co-rotating direction of the propellers (anticlockwise) and a relative phase angle of $\Delta\phi = 0°$. The propellers operated at a free-stream velocity (V_∞) of $30\,\mathrm{m\,s^{-1}}$ along the X-axis and at an advance ratio (J) of 0.8. The Mach number at the tip was 0.357, and the Reynolds number at the tip was 5.66×10^4. The simulation volume was a cubic box with side faces placed $64D$ away from the Global Reference System (GRS) origin. To prevent acoustic reflections at the outer boundary, an acoustic sponge was defined by two concentric spheres of radius $8D$ and $30D$ centered at the GRS origin [2, 16]. A total of 15 Variable Resolution (VR) regions were employed, with the finest VR region (VR14) having a resolution of 900 voxels per characteristic length (c_r). This resulted in the smallest voxel size of 1.79445×10^{-5} m. The acoustic data was sampled at $33.218\,\mathrm{kHz}$ on solid FW-H integration surfaces corresponding to the propeller blades, enabling high-fidelity noise analysis. In addition, a physical zig-zag trip was applied on the blade suction side to force turbulent boundary-layer transition, facilitating the transition from modeled- to resolved-scale modality (see Figure 1(c)). This approach minimized computational cost while accounting for relevant sources of noise [2, 4]. The acoustic data is captured at a sampling frequency of $33.218\,\mathrm{kHz}$ on the solid FW-H integration surfaces, which correspond to the propeller blades. This sampling frequency is chosen to ensure temporal discretization up to the tenth Blade Passing Frequency (BPF) harmonic, multiplied by a Nyquist factor of 3, thus mitigating aliasing artifacts. Subsequently, the Power Spectral Density (PSD) is computed using a single Welch block, filtered with a Hanning window to achieve a bandwidth of $\Delta f_r = 91.28\,\mathrm{Hz}$. The PSD of the far-field noise as a function of frequency f is calculated using the equation:

$$S_{pp}(f) = 10\log_{10}\frac{\mathrm{PSD(f)}}{p_{ref}^2},$$

where $p_{ref} = 20\,\mu\mathrm{Pa}$ is the reference pressure. The Sound Pressure Level (SPL) is defined as:

$$L_p(f) = 10\log_{10}\frac{\Delta f_r \mathrm{PSD(f)}}{p_{ref}^2},$$

allowing for the conversion of acoustic power spectral density into acoustic decibels (dB).

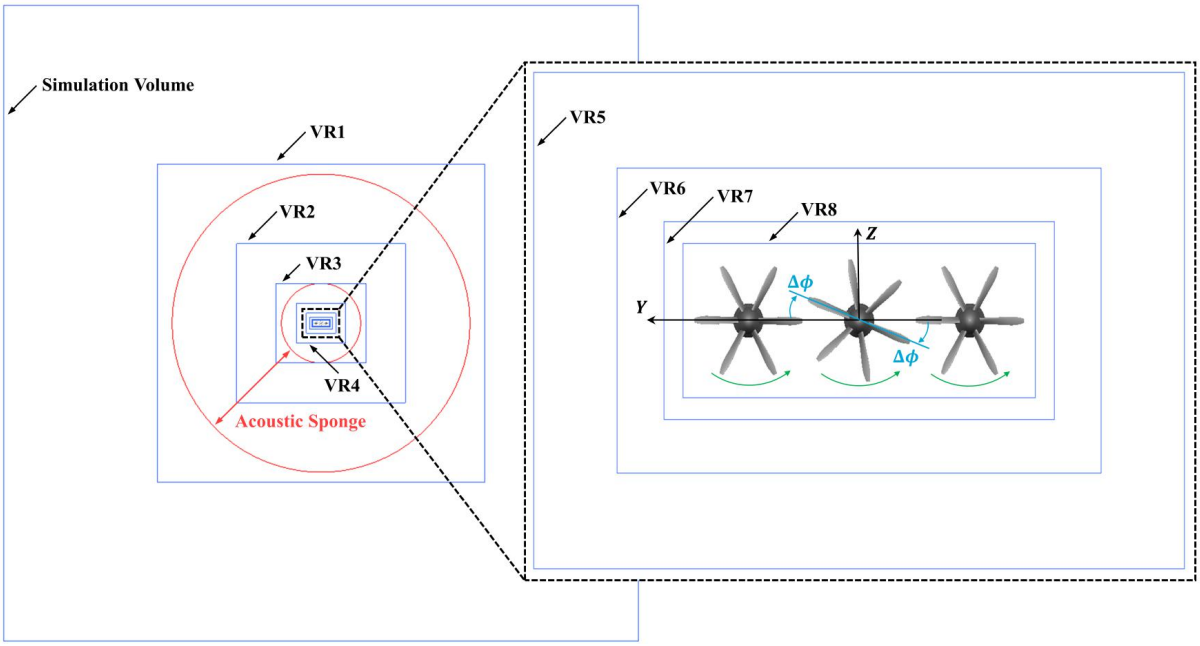

(a)

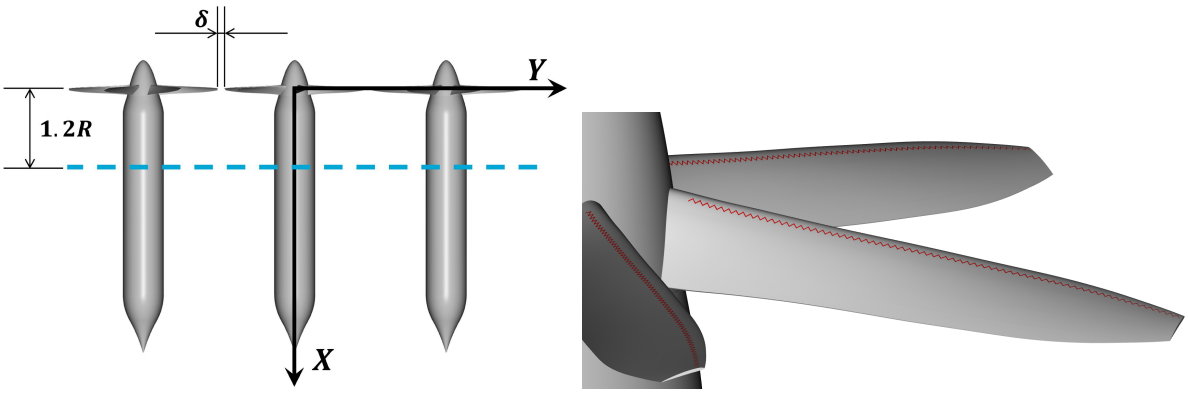

(b)

(c)

Figure 1: Figures borrowed from Ref. [24]: (a) Front view of the computational domain with the Variable Resolution (VR) mesh regions and the global reference frame. (b) Top view of the three adjacent propellers with wake survey plane location in a dashed line. (c) Close-up on the zig-zag trip applied on the blades.

2.2 Modeling of the unsteady sound sources

To model the unsteady interaction between the propellers, it is necessary to model the distribution of axial, radial, and tangential forces on the rotor disk, which are the essential ingredients for any sound prediction method based on the Ffowcs Williams and Hawkings (FWH) analogy [15]. In this work, we focus on the computation of the thrust distribution, leaving the tangential and radial forces to future developments, as explained below.

2.2.1 Definition of rigid helical vortex paths

The first assumption of the model being constructed lies in assuming that this unsteady interaction can be defined following the interaction between the slipstreams of the propellers. We model the slipstream of each blade as a helical vortical filament that begins its path from the tip of each blade. In Figure 2(a) a rigid system of six helical vortex paths has been plotted on top of the simulated wake of the isolated propeller, which can be visualized through the λ_2 criterion. It can be observed that the rigid helical paths overlap quite well with the simulated structures. As a first approximation, we assume that the induced velocity of the wake on the propeller is primarily due to this system of helical paths. We can notice from the same figure that, at least for this propeller with $J = 0.8$,

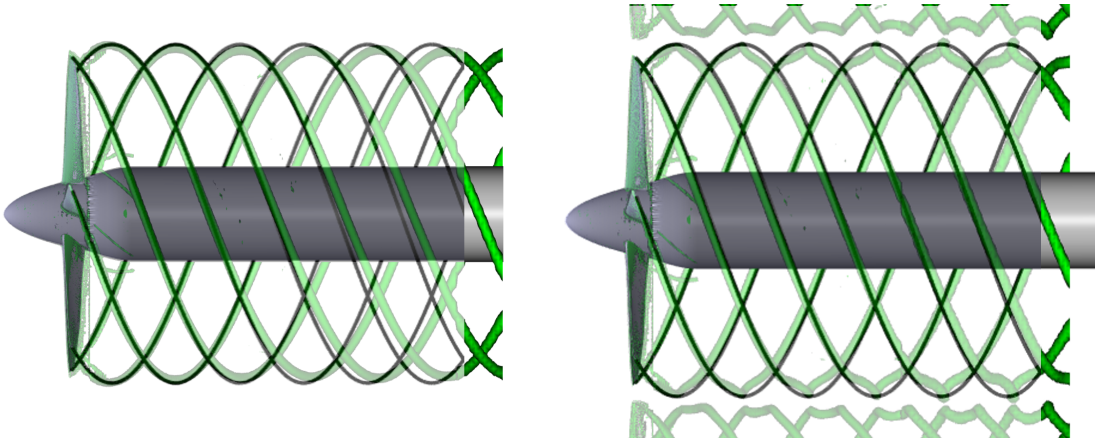

(a) (b)

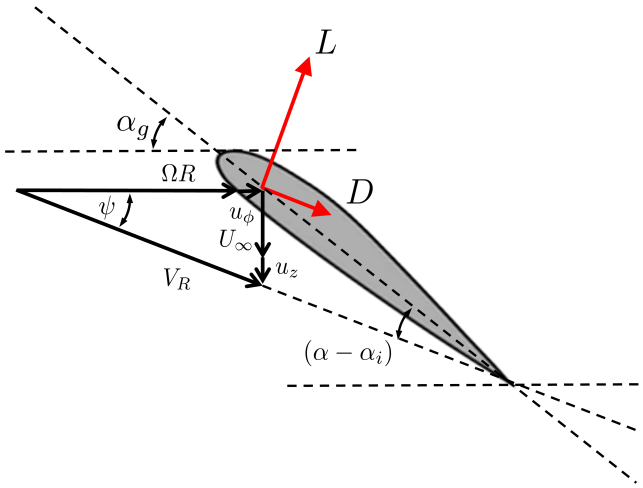

(c)

Figure 2: (a) and (b) illustrate the solid helical vortex paths overlapped with the isolated and installed propellers, respectively (vortex structures are visualized by means of λ_2-criterion, $\lambda_2 = -2 \times 10^6$ $1/\mathrm{s}^2$). (c) 2D spanwise element of the blade.

the stream contraction effect of the wake along the downstream direction becomes evident only far away from the rotor disk, and therefore, it is neglected in this study. This contraction effect is even less pronounced in the case of the propeller interacting with the two adjacent to it, hereinafter referred to as the installed propeller, as shown in Figure 2(b). Here we can also observe that when the simulated slipstreams approach each other, they are deformed without, however, breaking down or merging. Consequently, this deformation effect is also neglected for the model we are constructing. The helical step l_h, namely the axial distance covered by one helix loop, is defined by $l_h = U_D t_{\mathrm{rot}}$, where $t_{\mathrm{rot}} = 5.41867 \times 10^{-3}$ s, whereas $U_D = \frac{1}{2}(U_\infty + U_{\mathrm{exit}})$ is the axial velocity at the rotor disk [19]. In the same reference, for instance, we can find also the expression to define the exit velocity:

$$U_{\mathrm{exit}} = \sqrt{U_\infty^2 + \frac{T_{\mathrm{sim}}}{\frac{1}{2}\rho A_D}}, \tag{1}$$

where A_D is the rotor disk area, ρ is the air density, whereas $T_{\mathrm{sim}} = 18.05$ N is the isolated propeller averaged thrust. In this case, the used value comes from the simulations but, in a general case, the BEMT-computed thrust may also be used. The same value is used to define the helices for the adjacent propellers, considering the loss in performance due to the propellers' vicinity can be neglected, as demonstrated in [5, 24].

2.2.2 Biot-Savart law to compute the induced velocity field

To compute the induced velocity $\mathbf{U_i}$ everywhere in space induced by every helical vortex path, the Biot-Savart law is used [12]:

$$\mathbf{U_i} = \frac{\Gamma}{4\pi} \int_{\text{helix}} \frac{(\mathbf{l} - \mathbf{s}) \times d\mathbf{l}}{|\mathbf{l} - \mathbf{s}|^3}. \tag{2}$$

Here, $d\mathbf{l}$ is the helix element at point $\mathbf{l}$, which represents a position vector along the helical path of integration; $\mathbf{s}$ is the point at which the induced-velocity field is being computed. Γ is a constant representing the tip-vortex circulation: the computation of this constant is explained below. Equation 2 is discretized into 3000 segments per helical loop to allow numerical integration along the helical path[1].

2.2.3 Spanwise segmentation of the blade and thrust computation

Here, the link between the forces acting on each spanwise element and the induced velocity components is clarified. We follow the same reasoning that can be found in Ref. [19]. The blade is segmented into $N = 180$ spanwise elements, one of which is represented in Figure 2(c). For every spanwise element, we define the local lift as:

$$L = \frac{1}{2} \rho V_R^2 C_L c b, \tag{3}$$

where $c(r)$ is the local chord, dependent on the radial coordinate r, b is the spanwise element distance, $C_L \approx 2\pi(\alpha - \alpha_i)$. Here, α and α_i represent the profile angle of attack and induced angle of attack, respectively. We write $\alpha - \alpha_i = \alpha_g - \psi$, where $\alpha_g(r)$ is the local geometrical inclination of the airfoil chord element with respect to the rotor disk plane. The angle $\psi(r)$, also dependent on the radial direction, can be expressed as:

$$\psi = \tan^{-1}\left(\frac{U_\infty + u_x}{\Omega r + u_\phi}\right), \tag{4}$$

u_x and u_ϕ are the induced velocity components computed *via* Equation 2 in the axial and azimuthal direction, respectively (refer to Figure 2(c)). $\Omega = 1159.54$ rad s^{-1} is the angular velocity. The azimuthal coordinate ϕ is defined as positive in the anticlockwise direction, the same as the propeller revolution. The resultant velocity V_R, employed in Equation 3, is written as:

$$V_R = \sqrt{(\Omega r + u_\phi)^2 + (U_\infty + u_z)^2}. \tag{5}$$

Considering $B = 6$ blades and for every azimuthal position, the propeller thrust is computed as:

$$T \approx B \int_0^R L \cos(\alpha_g - \psi) dr. \tag{6}$$

2.2.4 Iterative process to compute the helical vortex circulation

The final step is to compute the circulation value Γ to exploit in Equation 2. We propose an iterative process, starting by computing the propeller thrust T_0 in Equation 6 imposing $\Gamma = 0$, thus $u_x = u_\phi = 0$. The value of T_0 corresponds to the particular case in which the propeller wake does not induce any influence on the generation of forces on the rotor disk, i.e., T_0 attains a maximum value. At this point, it is possible to proceed with an iterative process with respect to Γ, which concludes when the latter reaches a value necessary to match the thrust with T_{sim}. If one wishes, it would be possible to use as a target a thrust value calculated from BEMT-based calculations.

2.3 Rotating dipolar formulation

The tonal noise is computed from the blade loading using a rotating dipole model. This model relies on two underlying assumptions: *i)* the acoustic wavelength is much longer than the chord such that a blade segment is acoustically compact and *ii)* the noise production is dominated by forces on the blade in the axial and tangential direction, such that forces in the radial direction can be disregarded. With these assumptions, the noise production

[1] A convergence study is conducted and a plateau is reached with 3000 straight elements discretizing the helical path.

of the propeller can be modeled as a sum of rotating dipoles at different radii. This was introduced in [7] and the exact formulation used here is taken from [17]:

$$\hat{P}(mB\Omega) = \frac{-iB^2\Omega e^{-imB\Omega R_{\text{mic}}/a}}{4\pi R_{\text{mic}} a} \dots \sum_{p=-\infty}^{p=\infty} e^{-i(mB-p)(\phi-\pi/2)} J_{mB-p}\left(mBM\sin(\theta)\right)\left(m\cos(\theta)\hat{T}(p\Omega) - \frac{mB-p}{BM}\hat{F}_d(p\Omega)\right), \tag{7}$$

with $\hat{P}(\cdot)$, $\hat{T}(\cdot)$, $\hat{F}_d(\cdot)$ the Fourier transforms of the acoustic pressure at the microphone position, the thrust and the tangential force (drag) of a blade segment. m denotes the harmonic, B the number of blades, R_{mic} the microphone distance from the center of the propeller, a the speed of sound, and M the mach number of the blade segment. The angles ϕ and θ define the direction of the microphone and are indicated in Figure 3 (positive in the anticlockwise direction). The blades are divided into 100 blade segments of equal length in the radial direction, resulting in 100

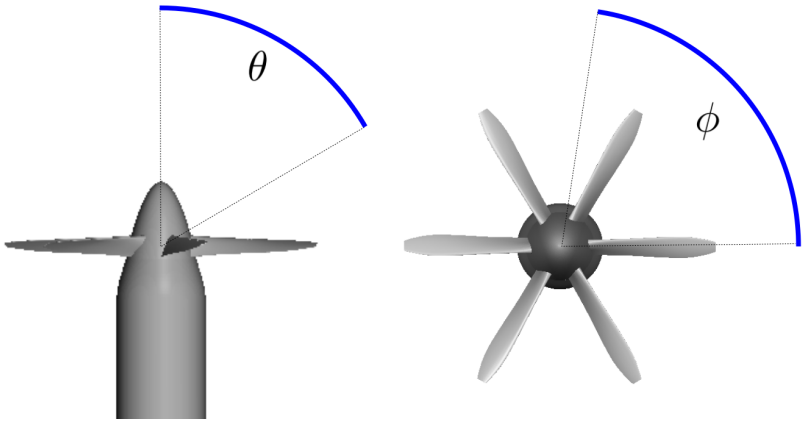

Figure 3: Definition of ϕ and θ that define the microphone direction.

discrete dipoles[2]. The forces on the blade segments are extracted in a time series from both the low-fidelity and high-fidelity (averaged over all blades and three full rotations) solutions. Then a Fourier transform is applied to obtain the harmonic contributions $\hat{T}(p\Omega)$ and $\hat{F}_d(p\Omega)$ with $-21 \geq p \geq 21$, which is sufficient to reach convergence for the 3^{rd} BPF (which corresponds to the 18^{th} harmonic of the shaft frequency).

3 Results

3.1 Acoustic code validation

The rotating dipolar formulation is validated with the blade-segment forces extracted from the high-fidelity data against the solid FWH formulation in the commercial tool PowerACOUSTICS 2022-HF01 (using data from 8 propeller rotations). The validation considers the middle propeller in a case where $\Delta\phi = -2°$. The microphones are at a distance of 20.32 m (100 diameters) from the center of the middle propeller to exclude any near-field noise contributions. Figure 4 plots the directivity of the 1^{st} BPF in the horizontal plane (i.e., $Z = 0$ m). A minor difference between the dipolar model and PowerFLOW can be observed. The difference mainly pertains to forces in the radial direction and thickness noise. When these are added to the dipole model the results give a near perfect match. For the middle propeller in directions where the noise is larger than 40 dB, the difference is smaller than 0.4 dB.

3.2 Modeled against simulated results

3.2.1 Unsteady thrust distribution

We apply the methodology presented in Section 2.2 to compute the thrust along the radial direction for the isolated propeller. In Figure 5(a), the latter is extracted directly from simulations for comparison. We observe that in both

[2]For the modeled case, N segments are used instead.

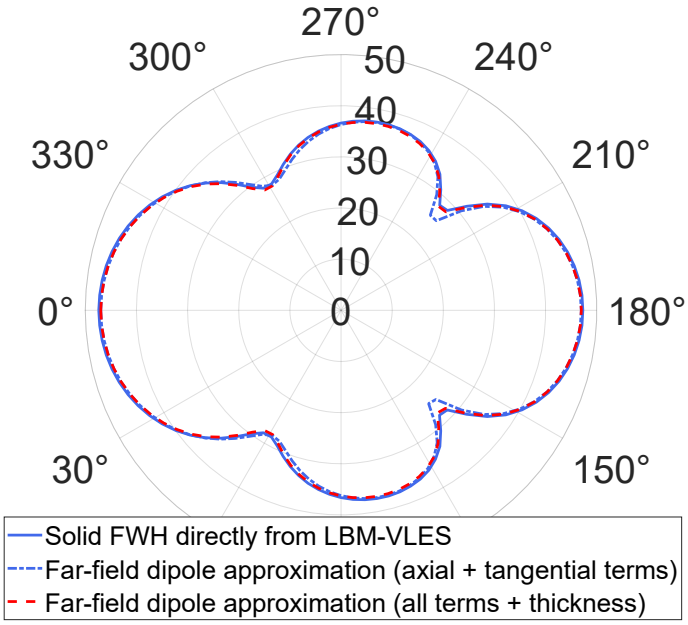

Figure 4: Validation of the dipole model.

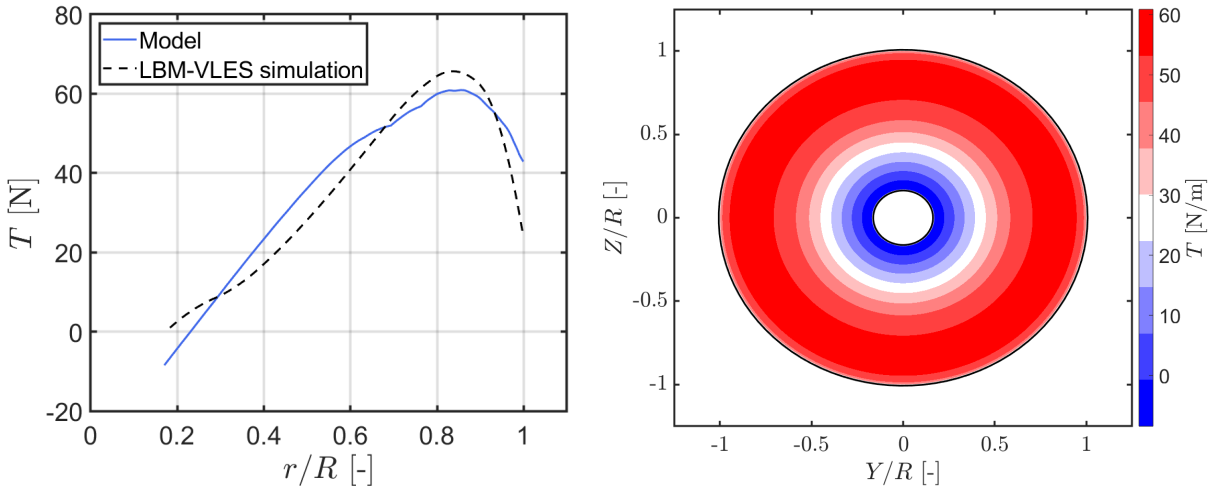

(a) (b)

Figure 5: Distribution of isolated thrust for modeled and simulated cases: (a) radial distribution at fixed azimuthal location; (b) azimuthal distribution.

cases, modeled and simulated, the peak of the curves occurs at $r/R = 0.84$, with a 9% relative difference (6 N). Noticeably, the modeled case does not exhibit the classical quadratic trend observed in the thrust originating from the simulations. Integrating the radial thrust distribution, we obtain that the blade of the isolated propeller produces the same thrust compared to the simulated case, as expected as a result of the iterative process to find Γ presented above. Consequently, considering the heavy assumptions made to model the thrust, we deem this result sufficiently satisfactory for this work. The radial thrust distribution shown in Figure 5(a) was calculated by fixing the azimuthal position. However, it is possible to discretize the azimuthal direction into N steps. At each of these steps, the blades and the rigid system of helical paths move azimuthally by $\phi + d\phi$. At this point, we repeat the methodology of Section 2.2 to obtain the azimuthal thrust distribution for the isolated propeller, shown in Figure 5(b). Obviously, in the case of the isolated propeller, the thrust distribution is azimuthally uniform. However, it is possible to add

the two adjacent propellers present in the simulation, taking into account their rigid system of helical paths as well. We can then calculate the radial and azimuthal distribution of thrust, considering the induced velocity not only from the propeller itself but also from the helical paths belonging to the adjacent propellers. We aim to visualize the effect of the induced velocity field on the thrust distribution, similar to what was done in Ref. [24]. To this end,

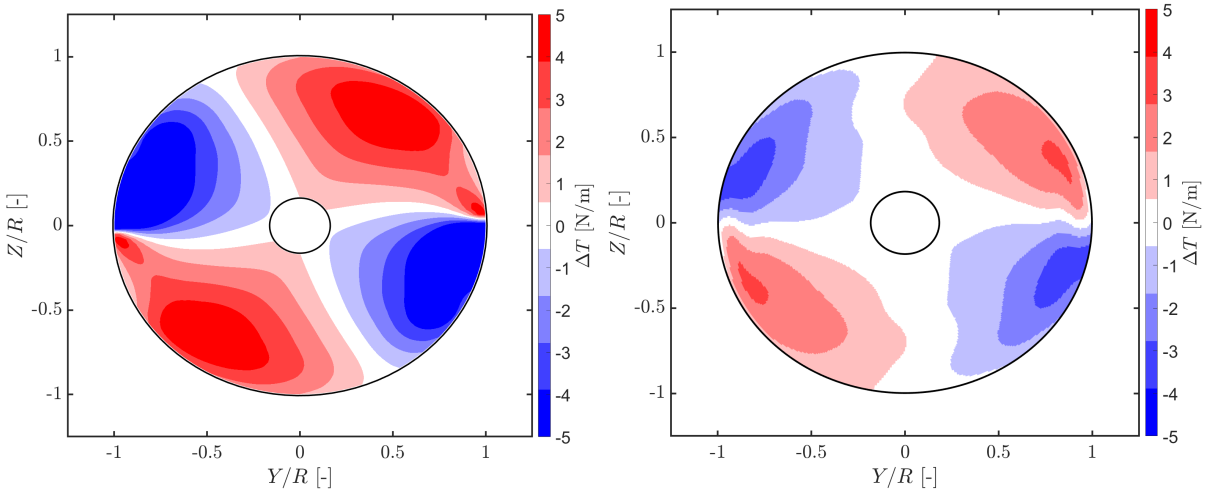

Figure 6: Unsteady thrust distributions (difference between the installed and the isolated propellers) for the modeled (a) and simulated (b) cases.

we show for the modeled case in Figure 6(a) the difference in thrust ΔT obtained by subtracting the thrust of the isolated case from that of the installed case. The latter should be compared with the analogous ΔT calculated from the simulations and reported in Figure 6(b). We can observe that both qualitatively and quantitatively, the modeled ΔT approximates the simulated one quite well. Indeed, the interactions between adjacent propellers are captured by the interaction between the systems of rigid helical paths.

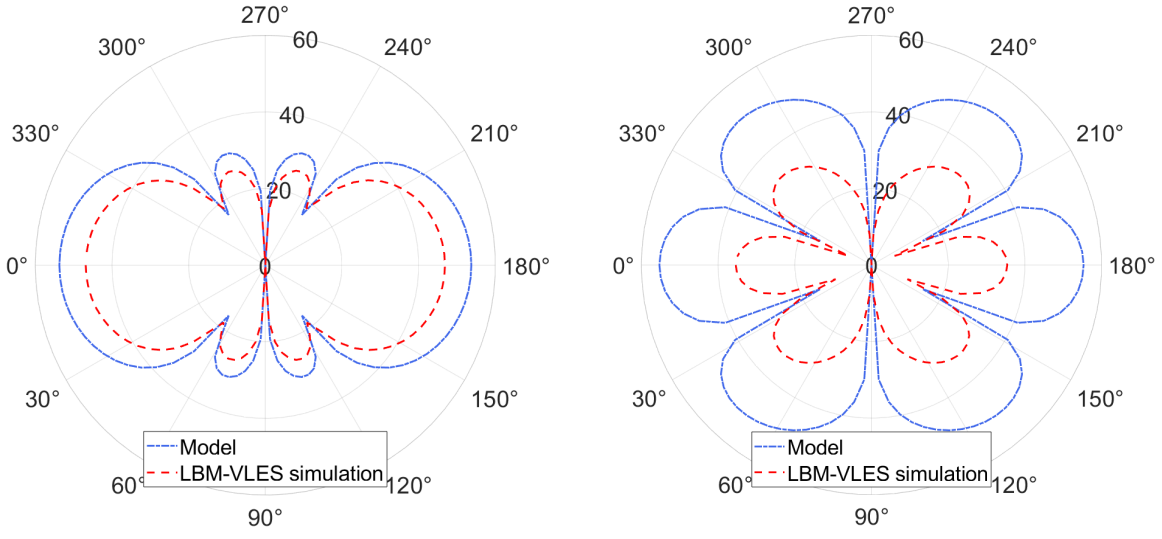

Figure 7: SPL tones computed for the first (a) and second (b) BPF harmonics and compared for the simulated and modeled cases.

3.3 Sound pressure level directivities

Using the unsteady thrust distribution calculated in Section 2.2, we compute L_p as discussed in Section 2.3. In Figure 7(a), we present the SPL of the first BPF harmonic calculated for a distribution of microphones lying perpendicular to the rotors' plane. Here, we show the comparison between the modeled and simulated cases. It can be observed that the shapes of the two directivities are identical; however, the amplitudes differ by up to 6 dB in front of and behind the propellers. In these positions, the unsteady loading noise contributes more significantly [24]. This difference is primarily due to the fact that we are not considering the actual lift coefficients, but the theoretical slope of 2π to calculate the thrust distribution shown in Figure 5(a). In the future, having the actual lift coefficients distributed along the blade, it will be possible to calculate a more realistic integral thrust value that reaches the same peak as the simulated one. In fact, the portions of the blade closer to the tip contribute more to the generation of sound due to higher local velocities. We can observe in Figure 7(b) the directivity calculated for the second BPF harmonic. Again, the shapes coincide; however, we observe a much larger difference in amplitudes, reaching a maximum of 20 dB also in this case in front of and behind the rotors. In this regard, examining Figure 6(a), one can notice the presence of 6 peaks in the unsteady thrust distribution: 2 in the negative direction of ΔT, and the other 2 in the positive direction. This does not occur in the case obtained through simulations, as can be seen in Figure 6(b). The 2 additional positive peaks, lying on $Z/R = 0$, can be attributed to the singular behavior of the vortices distributed along the helical paths and near the blade tip. This fictitious increase in periodicity along the azimuthal direction is responsible for the increase in amplitudes of the second harmonic tone of the BPF.

4 Conclusions

The presented study constitutes a step forward in understanding and modeling the complex interaction noise phenomena arising from distributed propulsion systems, particularly in the context of UAM. By investigating the interaction between adjacent propellers in a DEP configuration, this work provides a framework for developing noise prediction methods. Through high-fidelity simulations and the development of a low-fidelity modeling approach, the thrust distribution and its impact on sound radiation are modeled. The methodology employs the rotating dipole formulation fed by modeled unsteady thrust distribution, allowing for the prediction of tonal noise components resulting from the interaction between propellers. The modeling consists of approximating the slipstreams of propellers as rigid helical vortex paths and computing the induced velocity field, via the Biot-Savart law, which is the one that generates the unsteady loading on the rotor disk. The approach captures the essential aerodynamic interactions contributing to noise generation. Validation of the modeling approach against high-fidelity simulations demonstrates its potential in predicting SPL directivities, albeit with significant differences in amplitude. Improvements are planned for the future to overcome those. In particular, realistic lift and drag coefficients, calculated through a BEMT approach, will be employed to obtain a realistic thrust and tangential force distribution. It will be necessary to eliminate the singularities inherent to the vortical filaments by specifying a vortex finite core size as discussed, for instance, in Ref. [19]. Moreover, the model assumes that a change in the angle of attack of a blade section instantaneously results in a change in the force generated on it. However, as shown in the seminal work by von Kármán and Sears [21], lift and drag are also functions of the time derivatives of the angle of attack. It would therefore be desirable to add a more realistic response that incorporates a phase change in the azimuthal distribution of forces on the rotor disc. Nevertheless, despite the assumptions and approximations made, we believe that the developed model represents an interesting preliminary work. Indeed, in this study, the propellers are installed with a $\Delta\phi = 0°$, but it would nevertheless be easily possible to position them with different relative phase angles, thus being able to study their effect on noise emissions. Similarly, it would be possible to investigate the effect of the mutual distance between propellers in the axial direction or in the rotor plane. This is provided that the rigid helical paths proposed in this work continue to be approximately representative of the real slipstream distribution. This opens up the possibility of employing this model, whose calculation time remains on the order of one minute on a common laptop, for early-phase concepts when the designer needs to investigate numerous configurations and quickly estimate their tonal sound contributions.

Acknowledgements

The authors acknowledge receiving funding from the European Union's HORIZON Research and Innovation Actions programme under grant agreement number 101138209. The authors acknowledge Professor Christophe

Schram, von Karman Institute for Fluid Dynamics, for his help in the implementation of the rotating dipole formulation.

Declaration of competing interest

The authors state that they have no known competing financial interests or personal relationships that could have influenced the research presented in this study.

References

[1] Eduardo J. Alvarez and Andrew Ning. Modeling multirotor aerodynamic interactions through the vortex particle method. American Institute of Aeronautics and Astronautics, 2019.

[2] Francesco Avallone, Damiano Casalino, and Daniele Ragni. Impingement of a propeller-slipstream on a leading edge with a flow-permeable insert: A computational aeroacoustic study. 17(6):687–711, 2018.

[3] Nicholas K. Borer, Michael D. Patterson, Jeffrey K. Viken, Mark D. Moore, JoeBen Bevirt, Alex M. Stoll, and Andrew R. Gibson. Design and performance of the NASA SCEPTOR distributed electric propulsion flight demonstrator. In *16th AIAA Aviation Technology, Integration, and Operations Conference*. American Institute of Aeronautics and Astronautics, 2016.

[4] Damiano Casalino, Francesco Avallone, Ignacio Gonzalez-Martino, and Daniele Ragni. Aeroacoustic study of a wavy stator leading edge in a realistic fan/ogv stage. *Journal of Sound and Vibration*, 442:138–154, 2019.

[5] Reynard de Vries, Nando van Arnhem, Tomas Sinnige, Roelof Vos, and Leo L.M. Veldhuis. Aerodynamic interaction between propellers of a distributed-propulsion system in forward flight. *Aerospace Science and Technology*, 118:107009, November 2021.

[6] European Commission and Directorate-General for Mobility and Transport and Directorate-General for Research and Innovation. *Flightpath 2050: Europe's vision for aviation: maintaining global leadership and serving society's needs*. Publications Office, 2011.

[7] D. HANSON. *Near field noise of high tip speed propellers in forward flight*.

[8] Hyun D Kim, Aaron T Perry, and Phillip J Ansell. A review of distributed electric propulsion concepts for air vehicle technology. In *2018 AIAA/IEEE Electric Aircraft Technologies Symposium (EATS)*, pages 1–21. IEEE, 2018.

[9] Joseph Kummer and Thong Dang. High-lift propulsive airfoil with integrated crossflow fan. *Journal of Aircraft*, 43:1059–1068, 07 2006.

[10] H. Lee and D.-J. Lee. Rotor interactional effects on aerodynamic and noise characteristics of a small multirotor unmanned aerial vehicle. 32(4), Physics of Fluids, 2020.

[11] NASA. Strategic implementation plan: 2017 update. https://www.nasa.gov/sites/default/files/atoms/files/sip-2017-03-23-17-high.pdf, Washington, DC, 2017.

[12] Valery L. Okulov, Jens N. Sørensen, and David H. Wood. The rotor theories by professor joukowsky: Vortex theories. *Progress in Aerospace Sciences*, 73:19–46, 2014.

[13] Kyle A. Pascioni, Stephen A. Rizzi, and Noah Schiller. Noise reduction potential of phase control for distributed propulsion vehicles. American Institute of Aeronautics and Astronautics, 2019.

[14] Michel Roger. On Combined Propeller Synchronization And Edge Scattering For The Noise Reduction Of Distributed Propulsion Systems. page 8, ICSV26, Montreal, 2019.

[15] Michel Roger and Stéphane Moreau. Tonal-Noise Assessment of Quadrotor-Type UAV Using Source-Mode Expansions. *Acoustics*, 2(3):674–690, September 2020.

[16] Gianluca Romani, Edoardo Grande, Francesco Avallone, Daniele Ragni, and Damiano Casalino. Performance and noise prediction of low-reynolds number propellers using the lattice-boltzmann method. *Aerospace Science and Technology*, page 107086, 2021.

[17] Christophe Schram. Ffowcs Williams & Hawkings analogy. Lecture Notes, January 2011. Von Karman Institute for Fluid Dynamics.

[18] Alex M. Stoll, Edward V. Stilson, JoeBen Bevirt, and Percy P. Pei. Conceptual design of the joby s2 electric VTOL PAV. In *14th AIAA Aviation Technology, Integration, and Operations Conference*. American Institute of Aeronautics and Astronautics, 2014.

[19] J.N. Sørensen, V. Okulov, and N. Ramos-García. Analytical and numerical solutions to classical rotor designs. *Progress in Aerospace Sciences*, 130:100793, 2022.

[20] E. H. Jr. Teets, Casey J Donohue, and Patrick T Wright. Meteorological support of the helios world record high altitude flight to 96,863 feet. page 22, 2002.

[21] TH. VON KARMAN and W. R. SEARS. Airfoil theory for non-uniform motion. *Journal of the Aeronautical Sciences*, 5(10):379–390, 1938.

[22] Alessandro Zarri, Julien Christophe, Stéphane Moreau, and Christophe Schram. Influence of Swept Blades on Low-Order Acoustic Prediction for Axial Fans. *Acoustics*, 2(4):812–832, November 2020.

[23] Alessandro Zarri, Edoardo Dell'Erba, Wim Munters, and Christophe Schram. Fuselage scattering effects in a hovering quadcopter drone. In *28th AIAA/CEAS Aeroacoustics 2022 Conference*. American Institute of Aeronautics and Astronautics, 2022.

[24] Alessandro Zarri, Alexandros Koutsoukos, Francesco Avallone, Frits de Prenter, Daniele Ragni, and Damiano Casalino. Aerodynamic and acoustic interaction effects of adjacent propellers in forward flight. American Institute of Aeronautics and Astronautics, 2023.

[25] Teng Zhou and Ryu Fattah. Tonal noise acoustic interaction characteristics of multi-rotor vehicles. American Institute of Aeronautics and Astronautics, 2017.

[26] Wenwu Zhou, Zhe Ning, Haixing Li, and Hui Hu. An experimental investigation on rotor-to-rotor interactions of small UAV propellers. In *35th AIAA Applied Aerodynamics Conference*. American Institute of Aeronautics and Astronautics, 2017.